THE ASTROPHYSICAL JOURNAL, 449:880–887, 1995 August 20

ROSAT OBSERVATIONS OF SCATTERED X-RAYS FROM LMC X-4 IN ITS LOW STATE

JONATHAN W. WOO, GEORGE W. CLARK,[1] AND ALAN M. LEVINE
Center for Space Research, Massachusetts Institute of Technology, Cambridge, MA 02139
Received 1994 December 21; accepted 1995 March 1

ABSTRACT

Observations of the eclipsing accretion-powered high-mass X-ray binary LMC X-4 are described that confirm the idea that the low state of its 30.3 day period cyclical intensity variation is caused by a periodic blockage of the line of sight by a precessing accretion disk that is tilted with respect to the orbital plane of the binary. The principal evidence consists of the fact that the intensity and spectrum of scattered X-rays measured during total eclipse of the neutron star by the primary star are approximately the same in both the high and low states of the 30.3 day cycle. Therefore, the low state must be caused not by a decrease in the luminosity of the X-ray source but, rather, by total attenuation in intervening matter. Differences between the spectra observed in and out of eclipse in the high and in the low states are also consistent with the precessing disk hypothesis. The brightest of several flares detected in the low state had a peak intensity, which implies a source luminosity (0.2–2.5 keV) of 4×10^{39} ergs s^{-1} if the measured flux is interpreted as scattered and fluorescent radiation from the primary star's surface illuminated by the unblocked X-ray source. This peak luminosity is comparable to that previously reported for a flare observed in the high state. The flare also showed marginal evidence of the pulsar modulation, which is not inconsistent with the degree of spread in path lengths of the scattered radiation. The data also show that the column density to LMC X-4, derived by spectrum fits in both the low and high states, is about 4 times larger than the interstellar neutral hydrogen column density toward the LMC, possibly as a result of a circumstellar accumulation of matter from the wind of the primary.

Subject headings: accretion, accretion disks — binaries: eclipsing — stars: individual (LMC X-4) — X-rays: stars

1. INTRODUCTION

When the neutron star in a high-mass accretion-powered X-ray binary is eclipsed by the primary star, one can generally detect a residual intensity of X-rays that are the secondary Compton-scattered and fluorescent radiation from the stellar wind of the primary. Since the matter in the wind is widely distributed and broadly illuminated by the neutron star, it is reasonable to assume that the intensity of this secondary radiation is proportional to the intrinsic luminosity of the neutron star and, therefore, approximately constant. An interesting complication can arise if there is sufficient interstellar dust along or near the line of sight to give rise to grain-scattered X-rays that are delayed in arrival at Earth by virtue of their greater path lengths. The grain-scattered X-rays may then constitute a significant portion of the eclipse intensity in the form of an X-ray halo (Clark, Woo, & Nagase 1994, and references therein). In the case of an X-ray binary in the Magellanic Clouds, however, the column density of interstellar dust along the line of sight is so small that grain-scattered X-rays constitute a negligible fraction of the X-rays detected during an eclipse. Thus, essentially all the X-rays detected during an eclipse are secondary radiation, the intensity of which can be taken as a measure of the intrinsic luminosity of the eclipsed neutron star.

LMC X-4 is an eclipsing high-mass accretion-powered X-ray binary in the Large Magellanic Cloud with the properties listed in Table 1. Its intensity varies by a factor of ~ 60 between high and low states with a periodic cycle time of 30.3 days. This long-term variation, like the long-term variation of Her X-1, has been attributed to blockage of the direct X-ray beam by a precessing accretion disk that is tilted with respect to the orbit plane of the binary and periodically lies in a plane containing the line of sight to the neutron star (Lang et al. 1981; Priedhorsky & Holt 1987, and references therein). Dennerl et al. (1992) studied the long-term variation of LMC X-4 in the *ROSAT* All-Sky Survey data and in the *EXOSAT* data and concluded that the period is slowly decreasing. Features of the optical light curve have also been interpreted in terms of a precessing accretion disk (Ilovaisky et al. 1984; see also Heemskerk & van Paradijs 1989). A geometric model of the system has been devised by Heemskerk & van Paradijs (1989).

About once per day LMC X-4 exhibits a "flaring episode" during which the intensity increases sporadically by factors of up to ~ 20 for times ranging from ~ 20 s to 45 minutes (Epstein et al. 1977; White 1978; Skinner et al. 1980; Kelley et al. 1983; Pietsch et al. 1985; Dennerl 1989; Levine et al. 1991). The average spectrum ($E > 1$ keV) during a flaring episode is much softer than the average spectrum at other times.

In this paper we describe observations of LMC X-4 in and out of eclipse that prove that the low state of the long-term variation is caused by blockage of the line of sight to the neutron star as implied by the model of a precessing accretion disk. The observations also show changes in the X-ray spectrum in and out of eclipse and provide data on the intensity and modulation of a giant flare in the low state, which can be understood in terms of the model. The data also yield a measure of the thickness of circumstellar matter surrounding LMC X-4.

The observations are described in § 2, and the data analysis is given in § 3. Interpretation of the analysis and discussion of the binary properties of LMC X-4 are presented in § 4.

[1] Department of Physics, Massachusetts Institute of Technology, Cambridge, MA 02139.

TABLE 1

PARAMETERS OF THE BINARY SYSTEM LMC X-4

Parameter	Value	Reference
P_{orb}	1.40841 days	1
i_c (inclination angle)	57°– 65°	2
M_{opt}/M_X	10.6	2
θ_e (eclipse half-angle)	21°– 25°	2
R_0 (primary radius)	8.1 $R_\odot$	2
P_{pulse}	13.50 s	1
L_{opt}	6×10^{38} ergs s^{-1}	3
S_P	O7 III–V	3
A_V	0.16 mag	4
Distance	55 kpc	5

NOTE.—(1) Levine et al. 1991; (2) Woo 1993; (3) Hutchings, Crampton, & Cowley 1978; (4) van der Klis et al. 1982; (5) adopted.

2. OBSERVATIONS

We obtained data from two observations of LMC X-4 made with the Position Sensitive Proportional Counter (PSPC) in the focal plane of the X-ray telescope (XRT) of the X-ray observatory *ROSAT* (Trümper 1983). The PSPC-XRT system (Pfeffermann et al. 1987; Aschenbach 1988) was sensitive to X-rays in the energy range from 0.1 to 2.4 keV and had a field of view of 57′ radius. The energy resolution of the PSPC was 45% FWHM at 1 keV. The PSPC-XRT system efficiently rejected charged particle events and provided ~25″ angular resolution.

The first observation was carried out from 1991 October 28.6 to November 3.6 and yielded 46,000 s of useful data. Its purpose was to observe the northern part of the Large Magellanic Cloud; LMC X-4 was located about 40′ away from the image center (Bomans, Dennerl, & Kürster 1994). The second observation was from 1992 July 9.2 to 10.7 with a total exposure of 14,500 s with LMC X-4 close to the center of the field of view.

We estimated the phase of the long-term variation during each of the observations from the period and epoch given by Dennerl et al. (1992). These authors reported a light curve of LMC X-4 over ~40 days based on *ROSAT* sky survey data and found an epoch of maximum intensity (phase 0.0) of JD 2,448,226.0. They derived a period of $\sim 30.25 \pm 0.03$ days from a combined analysis of *ROSAT* and much earlier *EXOSAT* data. Using this ephemeris (which differs in the definition of zero phase from that of Lang et al. 1981), we found that the interval 1991 October 28.6 to November 3.6 corresponds to phases in the range from ~ -0.05 to ~ 0.15 with an uncertainty of ~0.01, which is in the high-intensity state of the cycle. The observation of 1992 July 9–10 spanned phases from 0.36 to 0.41 with an uncertainty of 0.02, during which LMC X-4 is in its low-intensity state.

3. DATA ANALYSIS AND RESULTS

For both observations, source counts were taken from a circular region centered on the image of LMC X-4, while background count rates in the source region were estimated from appropriately scaled count rates obtained in an annular region of the image surrounding the source region.

In the 1991 observation, the image of LMC X-4 was relatively large because of the off-axis aberrations of the XRT. We therefore defined the source region to have a radius of $r < 4.5$ around the image center of LMC X-4 and defined the background region by $6' < r < 8'$. Only events in pulse-height channels 20–249 (0.2–2.5 keV) were used. The source region data were corrected for background and then for vignetting using the exposure map of the entire observation.

For the 1992 observation, the source region was defined to have a radius of 1′ around the image center of LMC X-4, while background estimates were obtained from a source-free annulus defined by ($1.7 < r < 4.2$). Only events in pulse-height channels 20–247 (0.2–2.48 keV) were selected for the rest of our analysis. These selection criteria yielded an estimated background rate of 4×10^{-4} counts s^{-1} arcmin^{-2} keV^{-1} within this energy band, which is consistent with its being dominated by cosmic X-ray–induced events. The source region data were corrected for background, but no vignetting corrections were applied.

3.1. *X-Ray Light Curves and Pulsations*

The count rates in 216 s time bins for both the high- and low-intensity state observations are shown in Figures 1 and 2, respectively. In the high-intensity state the typical out-of-eclipse count rate was 6–8 counts s^{-1}, and the average in-eclipse count rate was 0.030 ± 0.006. The latter is about 0.5% of the out-of-eclipse intensity, which is consistent with the results from a previous observation of LMC X-4 with the *Ginga* satellite (Woo 1993).

During most of the observation in the low-intensity state the out-of-eclipse count rates were low (~0.1 counts s^{-1}) but nonetheless higher than the average in-eclipse count rate of 0.023 ± 0.004 counts s^{-1}. There were also two intervals of flaring activity lasting several thousand seconds during which the count rates increased suddenly, briefly, and sporadically. The flaring episodes are marked "FL01" and "FL02." Figure 2*c* displays the hardness ratio defined as the ratio of the count rates above and below 0.5 keV. The plot shows that the spectrum hardened during the flaring episodes.

The intervals containing flares are replotted in Figure 3 with finer time resolution. Figures 3*a* and 3*b* show several flares that consist of sudden increases in count rates to levels about 5 times the average between flares with durations of several hundred seconds. Similar flares were observed with *Ginga* (Levine et al. 1991). The strongest flare during the second episode is displayed in Figure 3*c* with a time resolution of 1 s. The peak count rate (~30–40 counts s^{-1}) was several hundred times the average count rate outside of the flaring episodes (~0.1–0.2 counts s^{-1}).

In Figure 2, we have marked the expected X-ray eclipse intervals with thick lines and the letters "EC." The average count rate around orbital phase 0.5 was approximately 6 times the average in-eclipse count rate.

A search for pulsations yielded evidence of periodic modulation with a statistical significance of about 2 σ in 200 s of data during the giant flare. The modulation is most significant at a trial period of 14.5 s.

3.2. *Spectral Analysis*

We constructed average background-subtracted pulse-height distributions (PHDs) from the uneclipsed high- and low-state data, in the following three categories: (1) data recorded during the flaring episodes displayed in Figure 2 (FL01 and FL02); (2) data recorded during the largest flare displayed in Figure 3*c*; (3) data not included either in category (1) or in the eclipses (EC). For each PHD in the energy range from 0.2 to 2.48 keV, we fitted a model PHD derived as a convolution of the PSPC response matrix with the following

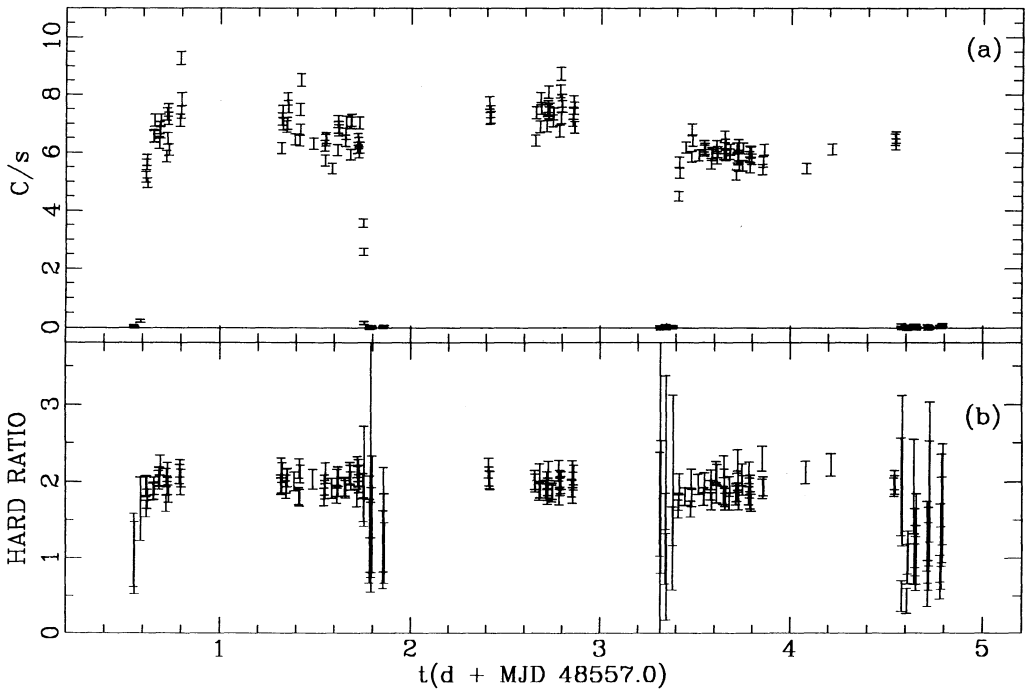

FIG. 1.—(*a*) *ROSAT* PSPC light curve of LMC X-4 (216 s bins) observed in the high-intensity state (1991 Oct 28.6–Nov 3.6). (*b*) The ratio of the count rate above 0.5 keV to that below 0.5 keV.

spectrum function expressed as photons cm^{-2} s^{-1} keV^{-1} and composed of an absorption factor multiplied by the sum of three component spectra: two power-law components and a Planck function:

$$I(E) = \exp\left[-\sigma(E)N_{\rm H}\right] \times \left[I_{\rm pl\,1}E^{-\alpha_1} + I_{\rm pl\,2}E^{-\alpha_2} + I_{\rm bb}\left(\frac{E}{E_{\rm bb}}\right)^2 \frac{(e-1)}{\exp\left(E/E_{\rm bb}\right)-1}\right]. \quad (1)$$

$I_{\rm bb}$ is the blackbody intensity at $E = E_{\rm bb}$, $I_{\rm pl\,1}$ and $I_{\rm pl\,2}$ are the power-law intensities at $E = 1$ keV, and e is the base of the natural logarithms. The shape parameters are the blackbody temperature $E_{\rm bb}$ and the power-law indices α_1 and α_2. The first power-law component represents the radiation from the accretion disk and is expected to be characterized by a higher value of α than the second power-law component. The second power-law component represents the radiation from the accretion column of the neutron star. Because of the falloff in sensitivity of the *ROSAT* PSPC-XRT above 2.5 keV, the power-law components were not well constrained. We therefore forced the index α_2 of the power law that we associate with the accretion column component to be 0.6, based on the previous *Ginga* observations of LMC X-4 (Levine et al. 1991; Woo 1993). The X-ray absorption cross section was assumed to be $\sigma(E) = \sigma_{\rm ph}(E) + 1.21\sigma_{\rm T}$, where $\sigma_{\rm ph}(E)$ is the photoelectric absorption cross section of cold matter given by Morrison & McCammon (1983), $\sigma_{\rm T}$ is the Thomson scattering cross section, and the factor 1.21 is the number of electrons per proton in the absorbing matter with normal cosmic abundances. A blackbody component with $E_{\rm bb} = 0.16$ keV was first detected in an analysis of *Einstein* solid state spectrometer observations of SMC X-1 by Marshall, White, & Becker (1983) and later in the analyses of *ROSAT* and *Ginga* observations of SMC X-1 by Woo et al. (1995).

For the spectrum fitting we rebinned the 256 channel PHDs accumulated from high-state data into 34 channels and the low-state PHDs into bins with at least 30 counts. The best-fit spectral parameters for the four average PHDs are listed in Table 2, and the fitted PHDs are shown in Figure 4.

From the optical extinction, $E(B-V) = 0.05 \pm 0.02$ mag, determined by Bonnet-Bidaud et al. (1981), the interstellar column density toward LMC X-4 is about 3×10^{20} H atoms cm^{-2} (Zombeck 1990). The absorption column densities derived from the spectral fits for all four spectra are much larger, which may signify a local accumulation of circumstellar matter.

3.3. *Monte Carlo Simulation*

To aid in the interpretation of the X-ray light curve, we carried out a Monte Carlo calculation of the propagation of X-rays through a spherically symmetric X-ray–ionized atmosphere with parameters adjusted to model the LMC X-4 primary star. The code was the same as that used in a previous study (Woo 1993). For the atmospheric density function we adopted the "hybrid" function from Clark et al. (1994):

$$n(r) = \frac{\Psi}{4\pi\mu r^2}\left\{1 + \left(\frac{r}{r_1}\right)^2\left(1 - \frac{r_0}{r}\right)^{\beta} \exp\left[-\frac{(r-r_1)}{h}\right]\right\} \times \left(1 - \frac{r_0}{r}\right)^{-\beta}, \quad (2)$$

in which $\Psi = \dot{M}/v_t$ represents the ratio of the mass-loss rate to the terminal velocity of the stellar wind. The quantity r_0 is an effective radius of the primary star that we set equal to the value 5.59×10^{11} cm. We adjusted the values of Ψ, β, r_1, and h, which were initially adopted from the *Ginga* LMC X-4 study (Woo 1993), to match the predicted light curve of the scattered photons in the Monte Carlo simulation with the observed X-ray light curve.

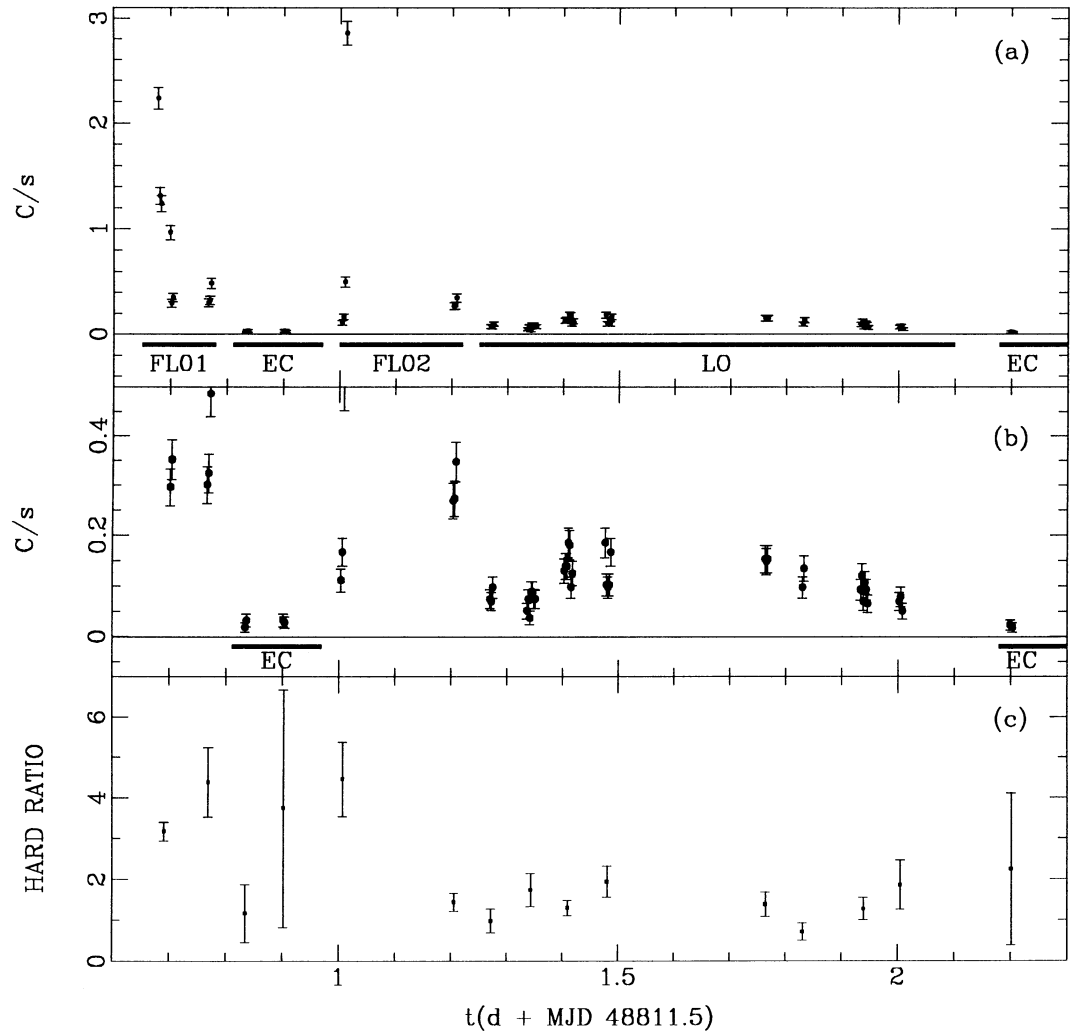

FIG. 2.—(*a*) *ROSAT* PSPC light curve of LMC X-4 (216 s bins). (*b*) The same light curve as in (*a*) but with an expanded count rate scale. (*c*) The ratio of the count rate above 0.5 keV to that below 0.5 keV. In (*a*) the time intervals that were used to construct the four spectra are shown: "FL01," "EC," "FL02," and "LO." Predicted eclipse intervals are marked as "EC" in (*b*).

We assumed that the photoelectric absorption cross section at a given location at a given energy is determined by the local ionization parameter $\xi = L_X/(nr^2)$. The local ionization parameter was calculated a priori by propagating the source spectrum through the atmosphere with the density function of equation (2). The Monte Carlo code launches 1 keV X-ray photons from the neutron star in random directions. Each photon is tracked in steps of 1/10 or less of a mean interaction length. At each interaction site, the photon may be Compton scattered or photoelectrically absorbed. If the photon is Compton-scattered, a new energy and direction for the scattered photon are calculated. If the photon is photoelectrically

TABLE 2

FITTED VALUES OF THE SPECTRAL FUNCTION

Parameter	High	Low	Flaring Episodes	Giant Flare
$N_H(10^{20}$ cm$^{-2})$	12.9 (0.7)	16.7 (12.7)	10.4 (7.1)	2.4 (0.5)
α_1	8.4 (0.4)	9.0 (6.7)	8.5 (5.3)	
$I_{pl\,1}$ (photons keV^{-1} cm^2 s^{-1})	4.2E−4 (1.7E−4)	0.17E−4 (1.32E−4)	0.13E−4 (1.11E−4)	
α_2[a]	0.6	0.6	0.6	0.6
$I_{pl\,2}$ (photons keV^{-1} cm^2 s^{-1})	0.0117 (0.0003)	1.26E−4 (1.87E−4)	0.0027 (0.0003)	0.023 (0.004)
E_{bb} (keV)	0.154 (0.003)	0.16 (0.12)	0.15 (0.02)	0.16 (0.02)
I_{bb} (photons keV^{-1} cm^2 s^{-1})	0.22 (0.02)	0.0020 (0.0081)	0.046 (0.046)	0.20 (0.02)
χ^2_ν	1.39	0.35	0.65	0.52
F_X[b] $(10^{-10}$ ergs cm^2 s$^{-1})$	0.99	0.016	0.17	1.75

NOTE.—The 1 σ uncertainties are quoted within the parentheses.

[a] The parameter value is fixed.

[b] For $0.2 < E < 2.5$ keV.

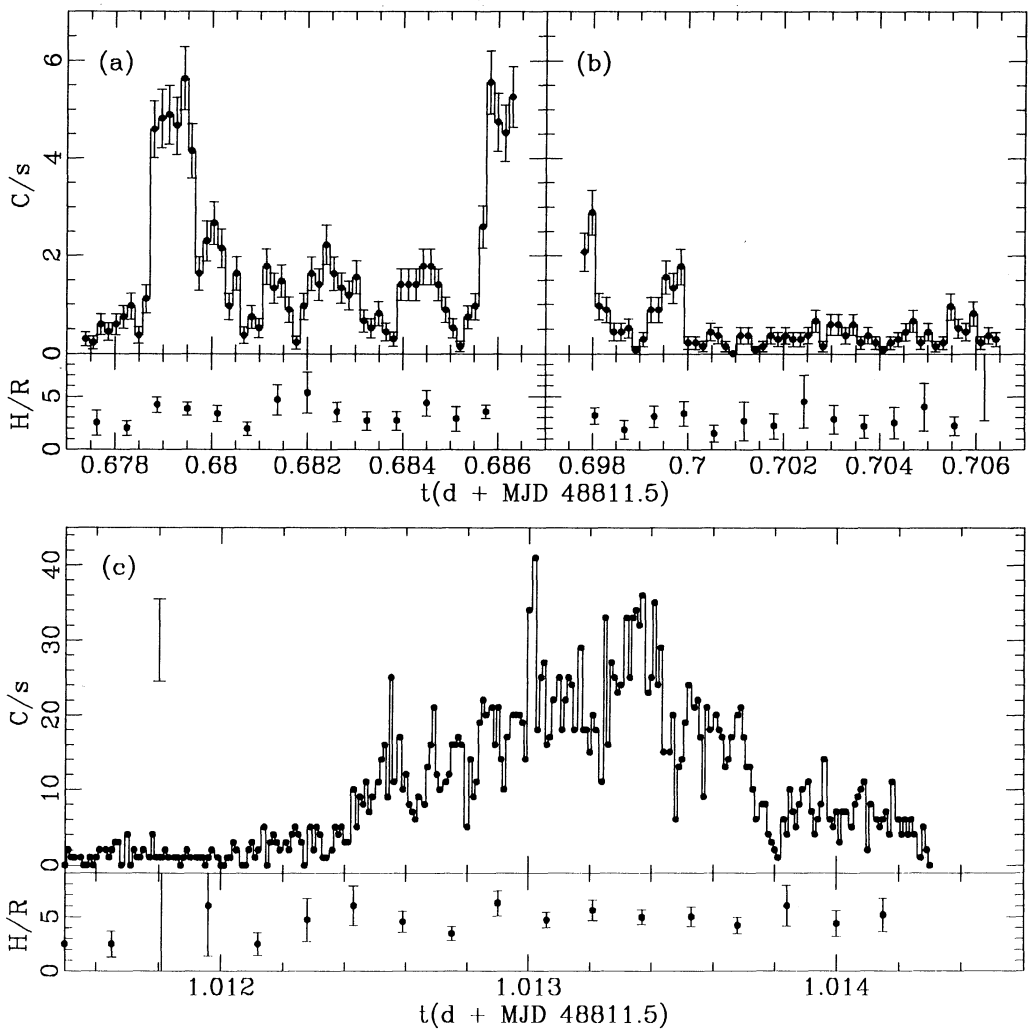

FIG. 3.—Details of light curves and hardness ratios during flares: (*a*) and (*b*) show 13.5 s data bins, and (*c*) shows 1 s data bins (to show short time variabilities). In (*c*), a typical $\pm 1\,\sigma$ error bar due to counting statistics is shown (for 30 counts s^{-1}).

absorbed, there may be fluorescent emission from iron or lower Z elements that are taken to be present with normal cosmic abundances.

The adjusted values of the hybrid density function parameters are $\Psi = 1.0 \times 10^{-10}\ M_\odot\ \mathrm{yr}^{-1}\ \mathrm{km}^{-1}\ \mathrm{s}$, $\beta = 1$, $r_1 = 1.41 r_0$, and $h = 2.82 \times 10^{10}$ cm.

Figure 5 displays the fraction of the 1 keV X-ray photons that are scattered at least once before escaping from the binary system. The scattering fraction varies from $\sim 0.5\%$ at the eclipse to $\sim 3\%$ around orbital phase 0.5. Out of eclipse the interactions are mostly Compton scattering from the stellar surface, so that the variation in the X-ray–illuminated area of the companion star visible from Earth produces an orbital phase–dependent intensity variation.

4. DISCUSSION

We have found that the X-ray intensities of LMC X-4 in eclipse during the low and high states are approximately the same. In striking contrast, the out-of-eclipse intensities differ by a factor of about 60 between the low and high states. Since the X-rays observed in eclipse are scattered from widely spread circumsource matter, their intensity provides a fair measure of the intrinsic luminosity of the neutron star. The similarity of the in-eclipse intensities in the high and low states therefore proves that the cause of the 30.3 day high-low cycle is not variations in the intrinsic X-ray luminosity of the neutron star. Instead, the cause must be periodic blockage of the line of sight to the neutron star. This conclusion is reinforced by the fact that the low-state out-of-eclipse intensity varies with orbital phase in a manner consistent with the Monte Carlo–calculated light curve of X-rays scattered by circumstellar matter and by the X-ray–illuminated surface of the primary star. Finally, the low-state out-of-eclipse spectrum is consistent with that expected for scattered and fluorescent radiation. All these results support the explanation of the long-term high-low variation of the X-ray intensity as the result of a periodic blockage of the line of sight by an accretion disk that is tilted with respect to the orbital plane and that precesses with the period of the high-low cycle.

Adopting a distance to LMC X-4 of 55 kpc, assuming isotropic scattering from circumstellar matter as the secondary source of X-rays observed during the low state, and using the measured flux cited in Table 2, we find the average luminosity (0.2–2.5 keV) of scattered radiation to be 5.8×10^{35} ergs s^{-1} during the uneclipsed, nonflaring low state. According to the Monte Carlo calculation (see Fig. 5), which assumes that the

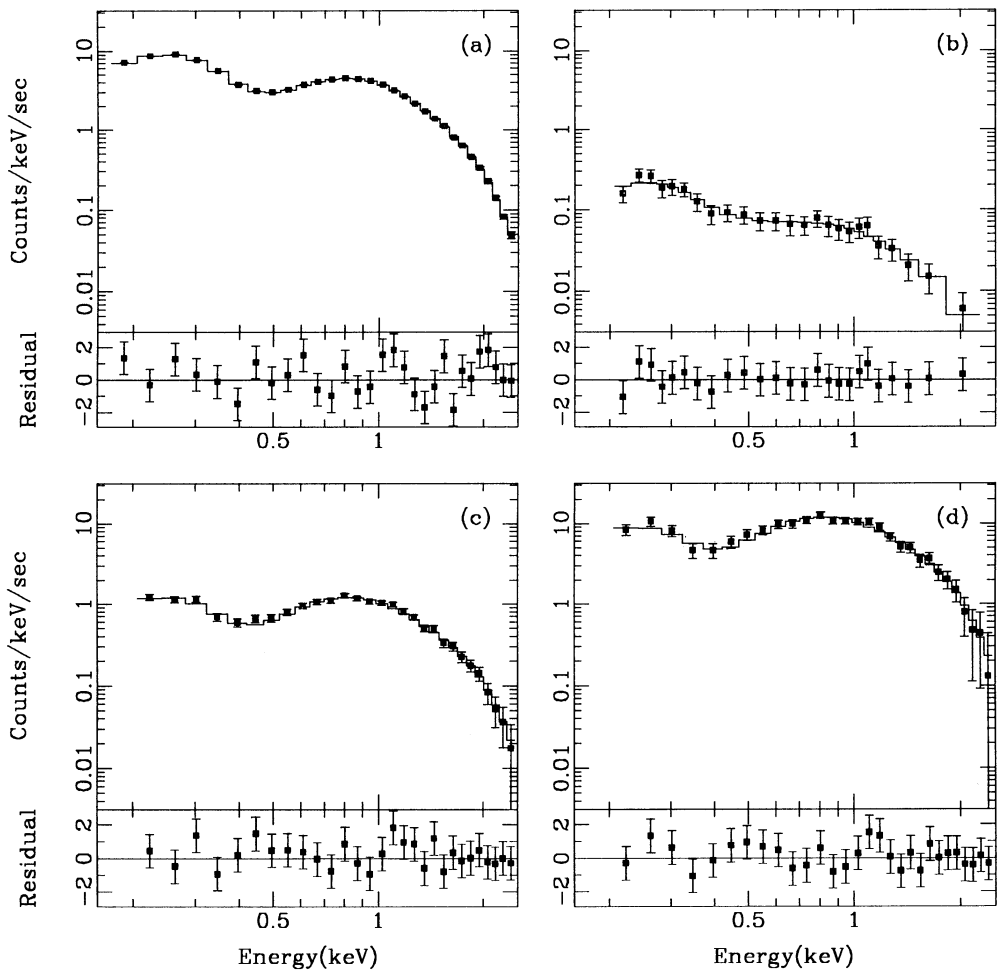

FIG. 4.—Pulse-height distributions of LMC X-4: (*a*) uneclipsed high state, (*b*) uneclipsed low state, (*c*) flaring episodes, and (*d*) the largest single flare (~200 s interval over flare shown in Fig. 3*c*). Histograms represent the best-fit pulse-height distributions.

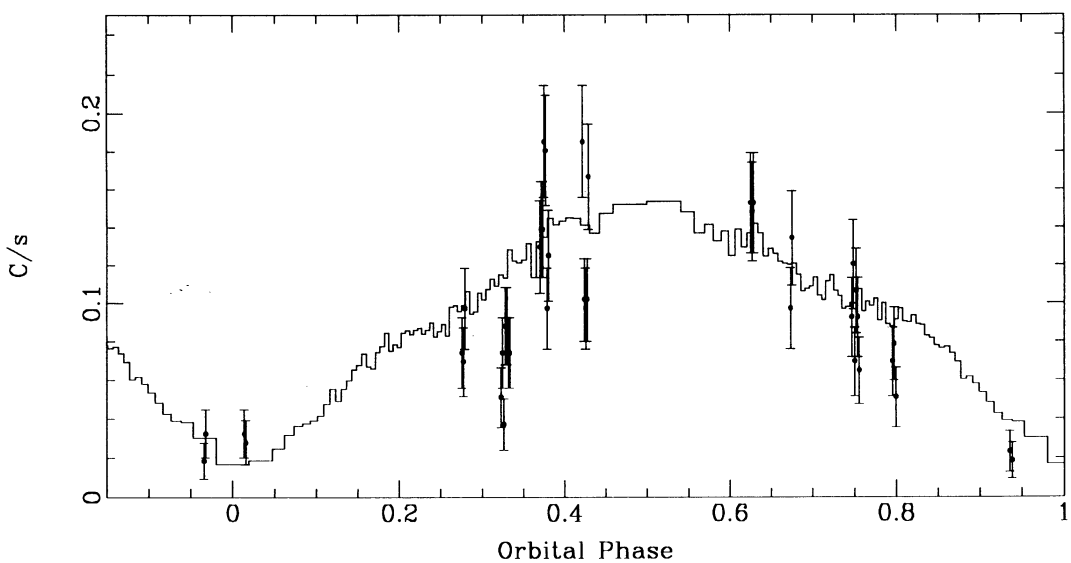

FIG. 5.—The observed count rates and predicted scattered-radiation light curve (*histogram*) that has been scaled to the observed light curve are plotted as a function of the orbital phase. A count rate of 0.1 counts s^{-1} corresponds to 2% of the unobscured direct intensity observed during the high state.

neutron star radiates isotropically, this luminosity is ~3% of the source luminosity; therefore, the implied intrinsic source luminosity must have been $\sim 2 \times 10^{37}$ ergs s^{-1}. At the peak of the giant flare (Fig. 3) the count rate is ~30 count s^{-1} or about 200 times higher than the count rate in the quiescent state (~0.15 count s^{-1} in Fig. 5). We can rule out the possibility that the flare X-rays were detected through the accretion disk because the measured column density is consistent with the circumstellar column density determined from the high-state data. It follows that the intrinsic source luminosity (0.2–2.5 keV) at the peak of the flare was approximately 4×10^{39} ergs s^{-1}, much larger than the Eddington limit. A similar high luminosity was found at the peak of a flare in the high state in a *Ginga* observation (Levine et al. 1991). Thus, the circumstellar matter responsible for scattering the X-rays in our direction must have been exposed to the full flare intensity of the neutron star.

If the apparent 14.5 s modulation in the giant flare data is real, then it must be a modulation in the intensity of the pulsar X-rays scattered from matter close enough to the line of sight to the neutron star to avoid complete smearing in time due to path length differences. When the neutron star is out of eclipse but hidden by the accretion disk, the surface of the primary is illuminated and, therefore, a source of albedo X-rays. The light travel time from the neutron star to the subsatellite point on the primary's surface is 11 s, comparable to the pulse period. Thus, it is reasonable to expect some remnant of the pulse modulation to be present in the scattered radiation. In fact, the giant flare occurred just after the neutron star emerged from eclipse so that only a thin crescent of the X-ray–illuminated surface of the primary was exposed to Earth. In that configuration the path length spread and the resultant reduction in the fractional pulse modulation are minimized. We note that the pulse fraction observed in the high state by *Ginga* (Levine et al. 1991) was ~0.5 during the intense flares compared to ~0.1 during quiescence. The apparent pulse fraction of ~0.2, which we obtain for the large flare in the low state, is smaller than in the previously observed high-state flares. The difference between the observed period and the intrinsic pulsar period may be an effect of the rapid changes of the source intensity during the flare or possibly a change in the beaming pattern as has been observed previously (e.g., Levine et al. 1991).

We note that changes in beaming pattern of the X-ray pulsar, as opposed to changes in luminosity, would not, except in very contrived situations, affect the scattered flux by a large factor. Therefore, the flares must be caused by large intrinsic changes in neutron star X-ray luminosity.

In a study of the distribution of circumstellar matter in a model of the high-mass X-ray binary SMC X-1, carried out by numerical three-dimensional hydrodynamic computation, Blondin & Woo (1995) demonstrated that X-ray heating of the primary star's atmosphere drives a thermal wind that constitutes most of the matter that populates the circumstellar environment. Quantitative estimates of the resulting column density of this circumstellar matter provided a plausible explanation for the excess of the column density to SMC X-1 over the interstellar column density derived from optical observations. The excess column density over the amount attributable to the interstellar medium in the present case of LMC X-4 also suggests an accumulation of circumstellar material from the wind of the primary star.

In thinking about possible future observations, we note that there is a large difference in the relative contributions to the spectrum of scattered X-rays observed in and out of eclipse from distant circumstellar matter and from matter near the primary's surface in systems like LMC X-4. Since the ionization state of the matter in these two scattering regimes may be quite different because of the difference in density and associated recombination rates, one can expect to observe differences in the relative intensities of the fluorescent lines in and out of eclipse, particularly during the low state when the direct beam is blocked. Such differences may be detectable with the improved spectrometry capabilities of future X-ray observatories and could provide interesting new information about the state and distribution of circumstellar matter in high-mass X-ray binaries.

The principal results of the present study can be summarized as follows:

In both the low and the high states of LMC X-4, the ratios of the in-eclipse intensities to the intensity at orbital phase 0.5 in the high-state were the same within the uncertainties of measurement and were approximately 0.005. In addition, the spectra out of eclipse in both the low and the high state were similar in shape.

The low-state out-of-eclipse intensity was ~3% of the high-state out-of-eclipse intensity. The low-state light curve is consistent with that predicted by a Monte Carlo calculation of scattering and fluorescence in the atmosphere and wind of the companion star, which is under X-ray illumination by the neutron star emitting at the same level of intrinsic luminosity as in the high state.

These results support the idea that the low-intensity state is caused by periodic blocking of the line of sight to the neutron star by an accretion disk that is tilted with respect to the orbital plane.

Two flaring episodes were observed, separated by ~10 hr. Individual flares showing count rate increases by at least 1 order of magnitude typically lasted several hundred seconds.

The column density to LMC X-4 determined from data accumulated during both low and high states is about 4 times larger than the interstellar column density of $N_H^{ISM} = 3 \times 10^{20}$ H atoms cm^{-2} inferred from optical measurements. The excess column density may indicate an accumulation of matter from the thermal wind driven from the surface of the primary star by X-ray heating.

This research was supported in part by grant NAG 5-1656 from the National Aeronautics and Space Administration.

REFERENCES

Aschenbach, B. 1988, Appl. Opt., 27, 1404
Blondin, J. M., & Woo, J. W. 1995, ApJ, 445, 889
Bomans, D. J., Dennerl, K., & Kürster, M. 1994, A&A, 283, L21
Bonnet-Bidaud, J. M., Ilovaisky, S. A., Mouchet, M., Hammerschlag-Hensberge, G., van der Klis, M., Glencross, W. M., & Willis, A. J. 1981, A&A, 101, 184
Clark, G. W., Woo, J. W., & Nagase, F. 1994, ApJ, 422, 336
Dennerl, K. 1989, in Proc. 23d ESLAB Symp., ed. J. Hunt & B. Battrick (Noordwijk: ESA-ESTEC), 39
Dennerl, K., Kuerster, M., Pietsch, W., & Voges, W. 1992, in Lecture Notes in Physics, Vol. 416, New Aspects of Magellanic Cloud Research, ed. B. Baschek, G. Klare, & J. Lequeux (Berlin: Springer), 74
Epstein, A., Delvaille, J., Helmken, H., Murray, S., Schnopper, H., Doxsey, R., & Primini, F. 1977, ApJ, 216, 103

Heemskerk, M. H. M., & van Paradijs, J. 1989, A&A, 223, 154
Hutchings, J. B., Crampton, D., & Cowley, A. P. 1978, ApJ, 225, 548
Ilovaisky, S. A., Chevalier, C., Motch, C., Pakull, M., van Paradijs, J., & Lub, J. 1984, A&A, 140, 251
Kelley, R. L., Jernigan, J. G., Levine, A., Petro, L. D., & Rappaport, S. 1983, ApJ, 264, 568
Lang, F. L., Levine, A. M., Bautz, M., Hauskins, S., Howe, S., Primini, S. A., Lewin, W. H. G., Baity, W. A., Knight, F. K., Rothschild, R. E., & Petterson, J. A. 1981, ApJ, 246, L21
Levine, A., Rappaport, S., Putney, A., Corbet, R., & Nagase, F. 1991, ApJ, 381, 101
Marshall, F. E., White, N. E., & Becker, R. H. 1983, ApJ, 266, 814
Morrison, R., & McCammon, D. 1983, ApJ, 270, 119
Pfeffermann, E., et al. 1987, Proc. SPIE, 733, 519
Pietsch, W., Pakull, M., Voges, W., & Staubert, R. 1985, Space Sci. Rev., 40, 371
Priedhorsky, W. C., & Holt, S. S. 1987, Space Sci. Rev., 45, 291
Skinner, G. K., et al. 1980, ApJ, 240, 619
Trümper, J. 1983, Adv. Space Res., 2, 241
van der Klis, M., Hammerschlag-Hensberge, G., Bonnet-Bidaud, J. M., Ilovaisky, S. A., Mouchet, M., Glencross, W. M., Willis, A. J., van Paradijs, J. A., Zuiderwijk, E. J., & Chevalier, C. 1982, A&A, 106, 339
White, N. E. 1978, Nature, 271, 38
Woo, J. W. 1993, Ph.D. thesis, MIT
Woo, J. W., Clark, G. W., Blondin, J. M., Kallman, T. R., & Nagase, F. 1995, ApJ, 445, 896
Zombeck, M. V. 1990, Handbook of Space Astronomy & Astrophysics (Cambridge: Cambridge University Press)